nature photonics

LETTERS

PUBLISHED ONLINE: 15 JULY 2012 | DOI: 10.1038/NPHOTON.2012.157

# All-optical wavelength shifting in a semiconductor laser using resonant nonlinearities

Julien Madéo[1], Pierrick Cavalié[1], Joshua R. Freeman[1], Nathan Jukam[1†], Jean Maysonnave[1], Kenneth Maussang[1], Harvey. E. Beere[2], David A. Ritchie[2], Carlo Sirtori[3], Jérôme Tignon[1] and Sukhdeep S. Dhillon[1*]

**For future ultrafast all-optical networks, new optical devices are required that can directly manipulate communication channels and shift their wavelength over the bandwidth of an optical fibre (50 THz)[1,2]. Solutions based on nonlinear processes have been proposed, but these suffer from having only low efficiencies as a result of low nonlinear susceptibilities[3]. Here, we demonstrate all-optical wavelength conversion of a near-infrared beam using a resonant nonlinear process within a terahertz quantum cascade laser[4]. The process is based on injecting a low-power continuous-wave near-infrared beam in resonance with the interband transitions of the quantum cascade laser. This results in an enhanced nonlinearity that allows efficient generation of the difference and sum frequency, shifting the frequency of the near-infrared beam by the frequency of the quantum cascade laser. Efficiencies of 0.13% are demonstrated, which are equivalent to those obtained using free electron lasers. As well as having important implications in its application in ultrafast wavelength shifting, this work also opens up the possibility of efficiently upconverting terahertz radiation to the near-infrared and enables the study of high terahertz-optical field interactions with quantum structures using quantum cascade lasers.**

Wavelength division multiplexing (WDM) is currently used extensively in optical fibre networks to enhance the carrier capacity of optical fibres where each wavelength in a multiwavelength bunch is assigned to a particular communication channel[5]. In these types of networks wavelength manipulation is essential for data routing, and optoelectronic shifters are used to perform wavelength shifting, where the optical signal is converted into an electrical signal and then back into an optical signal at a different wavelength. However, this process creates an undesirable speed bottleneck. To overcome this problem, as well as to increase the bandwidth, all-optical networks have been proposed to replace their electrical counterparts. For such types of network, new optical devices are therefore required that can directly manipulate communication channels to shift their wavelength across the optical fibre bandwidth.

Nonlinear processes in semiconductor devices have the potential to fill this technological gap, as two wavelengths in a nonlinear material can be mixed to generate a sum or difference frequency, effectively shifting the original wavelengths[3]. Normally, however, these techniques are based on the small bulk nonlinearities of the material and therefore demand phase-matching for a long interaction length and/or high pump powers. These considerations can be overcome using the resonant nonlinearities of quantum wells[6,7], which are orders of magnitude greater than those of the bulk, permitting much shorter interaction lengths. Indeed, there have been a number of investigations of the wavelength shift of a near-infrared (NIR) beam in the presence of an intense terahertz beam in a quantum well system[8–11]. These studies were based on enhanced nonlinear susceptibilities where the NIR beam was resonant with excitonic interband transitions and the terahertz beam was resonant with excitonic intersubband levels. The resonances could be modified to engineer the wavelength shift by changing the quantum well geometry[10] or by the application of an external electric field[12,13], and large efficiencies (0.1–0.2%) could be obtained[14,15]. However, an important factor to be taken into account when considering all this previous work is that the terahertz beam was provided by an entire facility—the free electron laser (FEL)—thus prohibiting its relevance to real-world applications.

The recently realized terahertz quantum cascade lasers (QCLs)[4,16] are semiconductor sources that operate in the terahertz range. The operation of QCLs is reliant on intersubband transitions, with the laser action taking place between confined conduction band subbands in a series of coupled quantum wells. The intracavity fields (up to a few kV $cm^{-1}$) of these devices can approach those used in the FEL studies mentioned previously[15]. QCLs therefore have the potential to be used as integrated wavelength converters, shifting an external NIR beam by the QCL frequency by providing (i) large intracavity powers and (ii) enhanced nonlinearity from the interband resonance of the NIR beam with the confined states. Previous work using QCLs and a NIR beam took advantage of the bulk second-order nonlinearity of GaAs to perform frequency mixing[17] or a double resonant process[18], but the efficiencies of the processes were limited ($10^{-4}$ to $10^{-3}$%). Here, we demonstrate a conversion efficiency of up to 0.13%, which represents an improvement of two orders of magnitude and is comparable to the values obtained in FEL investigations.

Figure 1a presents a schematic of the resonant nonlinear process, with the resonant interband excitation of the QCL with the NIR beam. The terahertz QCL laser transition $E_{QCL}$ occurs within the conduction band between the highlighted green states (green wave arrow). A NIR beam $E_{NIR}$ (red wave arrow) is coupled into the QCL cavity and resonantly tuned with an interband transition implying hole and electron states. As a result, a difference frequency $E_{NIR}-E_{QCL}$ is generated (dark red wave arrow) via a virtual state and a terahertz photon (green arrow), which is below the bandgap and therefore avoids absorption[10]. (The reverse situation also occurs with an excitation at the virtual transition to generate the sum frequency $E_{NIR}+E_{QCL}$ at the bandgap.)

Figure 1b shows the geometry of the experiment where the input interband excitation and the terahertz QCL emission are collinear, that is, in the same plane parallel to the surface of the QCL. This

[1]Laboratoire Pierre Aigrain, Ecole Normale Supérieure, UMR 8551 CNRS, Université P. et M. Curie, Université D. Diderot, 24 rue Lhomond, 75005 Paris, France, [2]Semiconductor Physics Group, University of Cambridge, JJ Thomson Avenue, Cambridge CB3 0HE, UK, [3]Matériaux et Phénomènes Quantiques, Université Denis Diderot–Paris 7, UMR 7162 CNRS, 75013 Paris, France; [†]Present address: Fakultät für Physik und Astronomie, Ruhr-Universität Bochum, 44780 Bochum, Germany. *e-mail: sukhdeep.dhillon@lpa.ens.fr

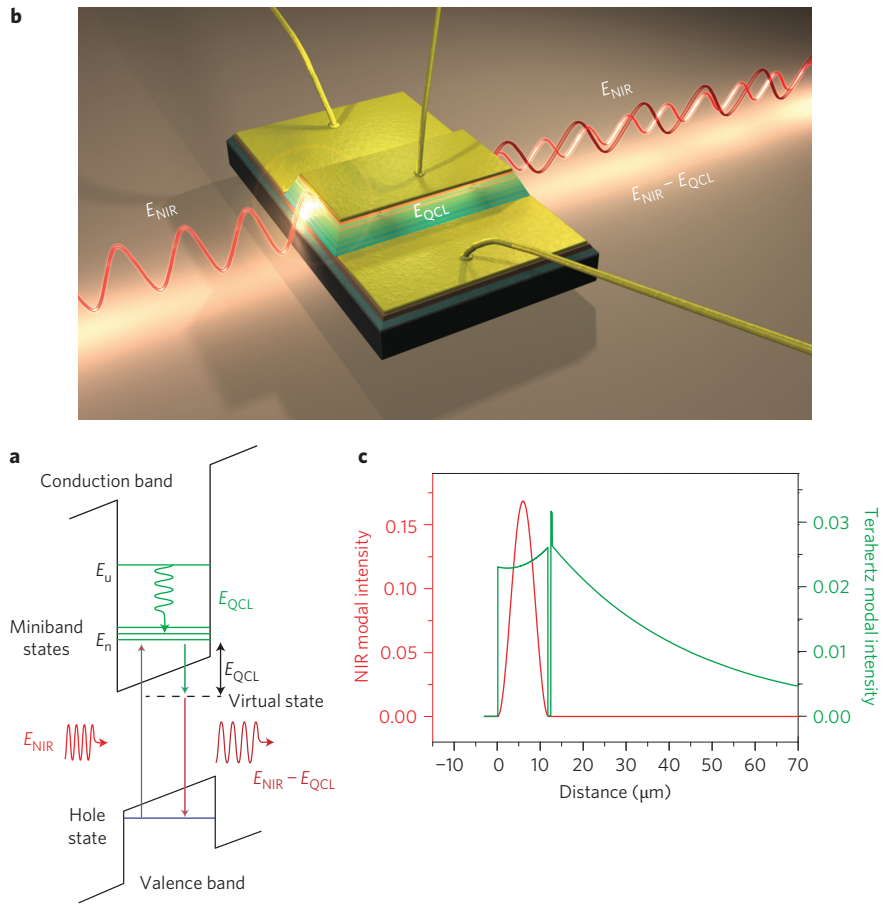


**Figure 1 | Scheme principle and optical modes. a**, Schematic of the resonant nonlinear process for the generation of difference frequency $E_{NIR}$–$E_{QCL}$ in a QCL operating at $E_{QCL}$ (green wave arrow between states $E_u$ and $E_n$). A NIR pump $E_{NIR}$ (red wave arrow) is tuned in resonance with interband transitions involving hole states in the valence band and electron states in the miniband of a QCL. This allows the generation of a lower-energy beam (dark red wave arrow) at $E_{NIR}$–$E_{QCL}$ via a virtual state below the material bandgap (dotted line) and the terahertz photon (green arrow). (For clarity the process is shown for one quantum well.) **b**, Schema of the geometry and experimental principle. A NIR beam, $E_{NIR}$, is coupled into the cavity of a QCL operating at $E_{QCL}$ through one facet (left side of the figure). The transmitted $E_{NIR}$ and the difference frequency $E_{NIR}$–$E_{QCL}$ are collected through the opposite facet. (Image by D. Darson.) **c**, Intensity profiles of the terahertz QCL mode at 2.8 THz (green line) and the NIR mode (red line) of the dual wavelength QCL waveguide. The NIR mode is confined between the metallic upper contact layer and an AlGaAs layer, ensuring a maximum overlap with the active region of the QCL.

is in strong contrast to previous experiments, which have investigated resonant nonlinear mixing with the terahertz beam and NIR excitation orthogonal to one another[10,12,15,18]. Our guided geometry for both the terahertz beam and input interband excitation allows the use of a much longer interaction length. The NIR pump is coupled into one QCL facet and the difference frequency exits the opposite facet together with the remaining input (the latter depending on optical losses).

The guided modes are shown in Fig. 1c for the terahertz QCL emission and the injected NIR beam (just below bandgap) using a dual wavelength waveguide. The confinement of the transverse magnetic (TM) polarized terahertz beam is based on a standard surface plasmon mode. The NIR excitation (transverse electric (TE) or TM) is confined by the top metal layer and a 300 nm $Al_{0.5}Ga_{0.5}As$ layer grown between the lower doped layer and the substrate. This layer has a lower refractive index than the surrounding material and therefore dielectrically confines the injected NIR beam.

QCLs operating at 2.8 THz using GaAs/AlGaAs quantum wells and based on a bound-to-continuum design[19] were used and operated in c.w. mode at 10 K. (See Methods for more details on the sample and experimental set-up.) Figure 2a presents the spectra of the beam without transmission through the QCL, with the pump beam centred at $E_{NIR} = 1.5267$ eV ($\lambda = 812$ nm), that is, just above the effective bandgap of the QCL and corresponding to electronic transitions between the first confined hole and electron states. The polarization of the NIR beam was chosen to be parallel to that of the QCL (that is, TM-polarized), implying interband transitions from only the light hole states[20]. Figure 2b shows the spectrum after transmission through the QCL, driven below laser threshold (black curve). $E_{NIR}$ is just visible, originating from a parasitic part of the beam that does not pass through the ridge. The situation changes drastically when the QCL is above threshold (red curve). The difference frequency is clearly observed at $E_d = E_{NIR}$–$E_{QCL} = 1.5152$ eV ($\lambda = 818$ nm), that is, separated from the pump $E_{NIR}$ by exactly the photon energy of the terahertz QCL ($f = 2.78$ THz) and below the bandgap of the material. A point to note is the high apparent conversion efficiency, with the difference frequency being 14 times more intense than the pump wavelength (taken as the ratio of the integrated signals of the pump and sideband). This is due to the sharp interband absorption. To estimate the actual conversion efficiency, defined as the ratio given by the power of the sideband divided by that of the input NIR pump $P_d/P_{NIR}$, the coupling efficiency of the pump needs to be determined. This was achieved by characterizing the transmission of the pump at an energy below the effective gap of the QCL where the interband losses are zero. This allows the determination of the NIR pump intensity coupled

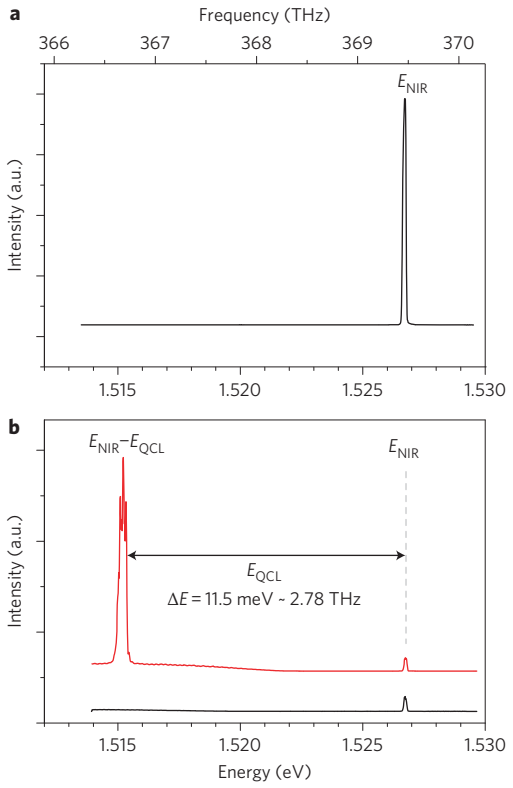


**Figure 2 | Wavelength shifting using interband excitation. a**, Spectrum of the NIR pump, $E_{NIR}$, before coupling into the QCL cavity. **b**, Spectrum of the transmitted beam with QCL below laser threshold (black curve) and spectrum of the transmitted beam with QCL above laser threshold (red curve). A high-intensity peak appears at $E_{NIR}$–$E_{QCL}$; that is, $E_{NIR}$ is shifted by the energy of the QCL frequency (2.78 THz).

into the input facet of the QCL. With this calibration, an efficiency of 0.13% is determined.

The inset of Fig. 3a demonstrates the appeal of this technique for terahertz detection. A high-resolution spectrum of the sideband (with the pump at 1.528 eV) with many modes is shown, and is an exact replica of the QCL Fabry–Pérot emission (and was taken in less than a second). This shows that this wavelength conversion allows one to measure and upconvert the terahertz emission of the QCL to the NIR. Furthermore, these measurements used standard charge-coupled device (CCD) camera technology for detection. The spectrum exhibits a resolution of 1.2 GHz, which is comparable to that of a considerably slower high-resolution Fourier transform infrared (FTIR) spectrometer.

The resonant nature of the interaction can be seen in Fig. 3a, which shows spectra for several pump wavelengths together with their corresponding difference frequencies for TM pump polarization. For clarity, the curves have been normalized by setting the pump wavelength intensities to one. As the pump energy is increased from 1.522 eV to 1.534 eV, the difference frequency initially increases in intensity, showing a double resonance before decreasing at higher pump energies. These results are summarized in Fig. 3b, which shows the efficiency with the absorption of the pump taken into account (see above) as a function of pump energy (square symbols). Resonances at 1.531 eV and 1.527 eV are observed, with the latter showing a conversion efficiency of 0.13%, which was the highest obtained. This is more than two orders of magnitude greater than previous demonstrations using QCLs. The full-width at half-maximum (FWHM) of each resonance was ~1–2 meV. These resonances arise when $E_{NIR}$ is resonant with interband transitions that have a large overlap between the electron and hole wavefunctions. Also shown in Fig. 3b is the efficiency obtained with a TE-polarized NIR beam corresponding to interband excitation predominantly from heavy holes states[20]. One resonance is clearly observed at 1.525 eV, and another broader one around 1.528 eV. The slightly lower energy of the resonance for TE polarization compared to that of TM polarization is due to the higher confinement of the heavy hole states, while the slightly reduced efficiency in TE polarization is due to the smaller overlap of the electron and heavy hole states.

To identify the states involved in the nonlinear process, photoluminescence from the QCL was investigated (Fig. 4b). As the photoluminescence emission is provided by the transitions with the lowest energy, that is, involving heavy holes states, it is compared to the

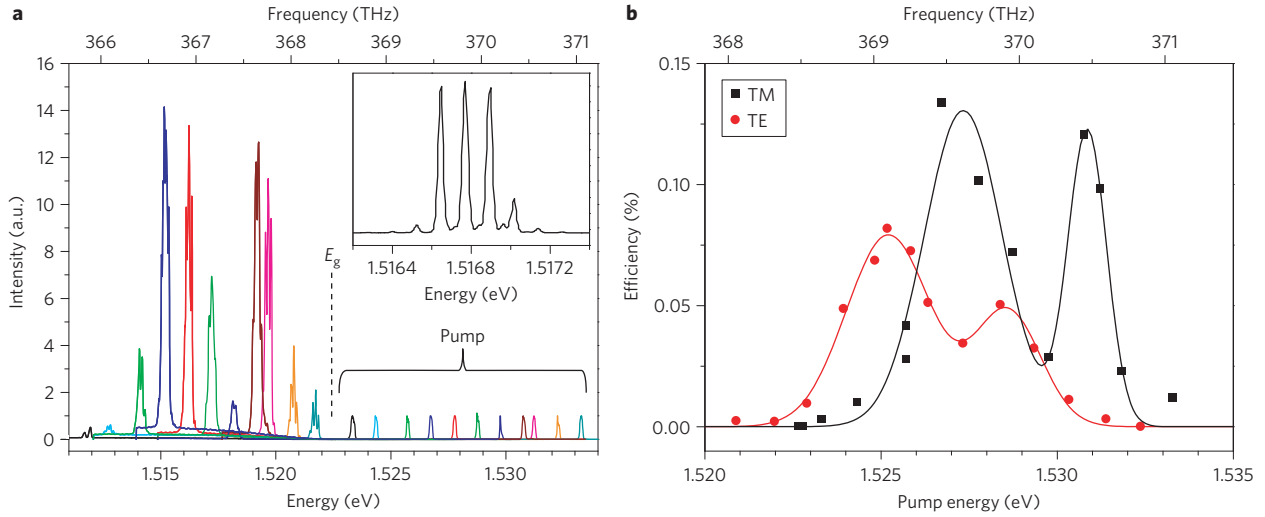


**Figure 3 | Resonant behaviour and polarization effect of the NIR pump. a**, Spectra of QCL output for different pump excitation energies. Pump beams are normalized to 1. $E_g$ corresponds to the energy from which the NIR pump is absorbed, showing that the generated beam is always below the absorption edge. Inset: high-resolution spectrum of the generated beam, which corresponds to the QCL emission intensity spectral profile. **b**, Conversion efficiency as a function of NIR pump energy, with losses taken into account for TE polarization (red circles) and TM polarization (black squares) of the input pump beam. Solid curves are Gaussian fits to the data.

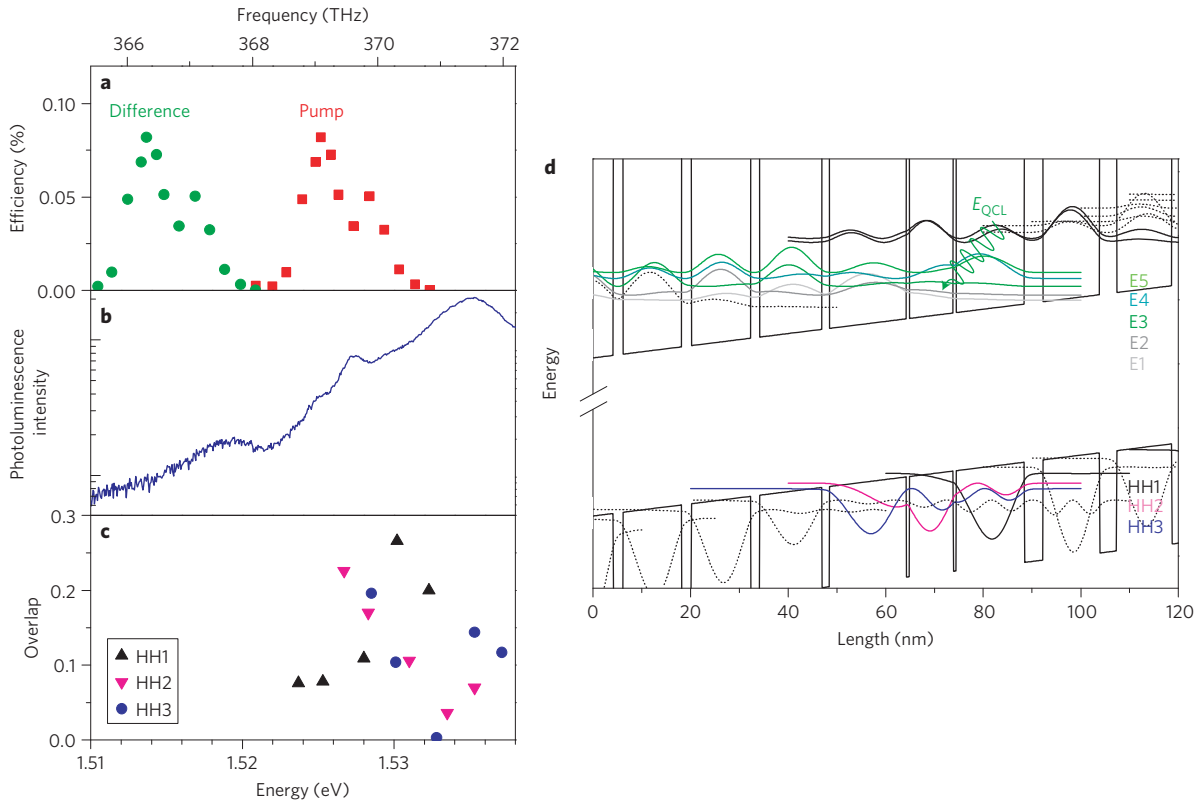


**Figure 4 | Confined states involved in resonant nonlinear interaction. a**, Conversion efficiency for TE polarization of the NIR pump as a function of the generated difference beam energy (green circles) and the pump energy (red squares). **b**, Photoluminescence spectrum of the QCL biased above laser threshold (that is, for wavelength shifting). **c**, Overlaps of interband transitions involving the three lowest-lying heavy holes states (HH1, HH2 and HH3) and the electronic states of the lower miniband of the QCL (E1 to E5). **d**, Band structure of the QCL showing the valence (heavy holes) and conduction band states. States in bold lines are those with significant overlap in the range of energies where the difference frequency is observed. Calculated overlaps in **c** correspond to transitions between HH1 (black), HH2 (magneta) and HH3 (blue) with miniband states increasing in energy from E1 to E5. The QCL laser transition is represented by a green wave arrow between the upper and lower laser states.

efficiency curve for TE polarization of the NIR pump (Fig. 4a, red squares). The TE efficiency is also plotted as a function of the difference energy $E_{NIR}$–$E_{QCL}$ (green circles). Regarding the resonances in the efficiency at the pump beam energies (red squares), the main peak corresponds to the shoulder in the photoluminescence spectrum at 1.525 eV and the higher-energy and broader resonance corresponds to a transition around 1.527 eV. Furthermore, no peaks are observed in the photoluminescence in the difference energy range (green circles), illustrating that there are no resonant transitions and confirming that the wavelength conversion is realized through a virtual state below the bandgap. (The small shoulder at 1.519 eV is due to photoluminescence from the GaAs substrate.) Figure 4c presents a comparison of the photoluminescence spectrum and the overlap of the interband wavefunctions of the QCL, the photoluminescence being proportional to the square of the overlap between the electron and hole states[21,22]. In Fig. 4d, the band structure of the studied sample is shown, including conduction and valence bands. The states that have a significant overlap in the energy range considered are highlighted and are the three lowest-lying heavy hole levels (labelled H1 to H3) and the five electronic states in the miniband (labelled E1 to E5). Comparing Fig. 4a,b,c, the efficiency peak at 1.525 eV is a result of resonances with HH1E1 and HH1E2 transitions, that is, the lowest-lying states. The higher-energy broader resonance is more difficult to identify with a single transition and appears to be linked to multiple contributions from the three hole states and the lower electron states. This explains the broader nature of the second resonance. A similar analysis performed for the light hole states shows a significant overlap only between the lowest-lying hole state and the lowest electronic states, which are separated by 3 meV, in agreement with the results of Fig. 3b. Thus, the nonlinear process is singly resonant with the lowest-energy hole states and the electronic states of the miniband of the QCL.

It is possible to estimate the second-order susceptibility, $\chi^{(2)}$, from the efficiency $\eta$ (refs 23–25):

$$\eta = \frac{P_d}{P_{NIR}} = \frac{8\pi^2 |\chi^{(2)}|^2 L^2 P_{QCL}}{\varepsilon_0 n_{NIR} n_{QCL} n_d c \lambda_d^2 S} e^{-\alpha_p \frac{L}{2}} \frac{\sin^2\left(\frac{\Delta kL}{2}\right) + sh^2\left(\alpha_p \frac{L}{4}\right)}{\left(\frac{\Delta kL}{2}\right)^2 + \left(\alpha_p \frac{L}{4}\right)^2} \quad (1)$$

where $P_d$ ($n_d$), $P_{NIR}$ ($n_{NIR}$), $P_{QCL}$ ($n_{QCL}$) are the intensities (refractive indices (~3.6)) of the generated beam, the input NIR pump and the terahertz QCL, respectively, $L$ is the cavity length of the QCL (1.5 mm), $\lambda_d$ is the generated wavelength (818 nm) and $S$ is the interaction area defined as the modal overlap between the three interacting waves (8,000 $\mu m^2$)[17]. The intracavity terahertz power is 75 mW, estimated from the detected output power and a facet reflectivity of 0.32. $\alpha_p$ represents the losses of the NIR pump (estimated at 1,000 $cm^{-1}$)[20] and $\Delta k$ is the phase mismatch. The losses of the difference frequency and the terahertz beam are taken to be zero. Although phase matching in the geometry presented here is possible

due to refractive index dispersion at resonance[26] (Supplementary Section S2), the high losses of the pump beam is the limiting factor regarding the interaction length. Equation (1) can then be simplified as

$$\eta = \frac{P_{\mathrm{d}}}{P_{\mathrm{NIR}}} \approx \frac{64\pi^2 \left|\chi^{(2)}\right|^2 P_{\mathrm{QCL}}}{\varepsilon_0 n_{\mathrm{NIR}} n_{\mathrm{QCL}} n_{\mathrm{d}} c \lambda_{\mathrm{d}}^2 S \alpha_{\mathrm{p}}} \frac{1}{\alpha_{\mathrm{p}}}$$

Taking the maximum efficiency of 0.13%, a second-order nonlinearity of $\sim 1 \times 10^4$ pm V$^{-1}$ can be determined. This is rough agreement with previous studies, which have shown interband nonlinearities in the range $10^2$ to $10^4$ pm V$^{-1}$ for quantum wells[27,28], confirming that the nonlinear susceptibility is enhanced by the resonant excitation. (This rather large range in simulated and experimental nonlinearities is a result of interband nonlinearities being a complex problem that involves the contribution of many real and virtual band-to-band transitions[28].)

We have shown that the resonant interband properties of a QCL can be used for efficient frequency mixing by making use of enhanced nonlinearities. The perspectives on this work are wide ranging. The wavelength shift can be engineered to any desired terahertz value[29] and can be applied equally to mid-infrared (MIR) QCLs[30], where the wavelength shift is much greater and can be used to shift between different telecommunication bands[31]. As well as providing room-temperature and high-power output[32], MIR QCLs are based on InGaAs/AlInAs quantum wells, for which the interband transition is directly in the telecommunication range. Further increases in efficiency could be realized through (i) adapted active region design or the insertion of passive quantum wells to enhance the nonlinearity through optimization of the overlaps between the confined states and (ii) the combination of intersubband nonlinearities with those of the interband transitions. This work also shows the potential to efficiently upconvert QCL emission, allowing the use of NIR technology for the detection of terahertz emission or providing a NIR–terahertz link for free-space telecommunications. On a more fundamental level, this work also opens up the possibility of studying high terahertz–optical field interactions using compact and powerful QCLs, research that was previously limited to entire facilities such as the FEL.

In conclusion, an efficient wavelength converter based on a compact QCL has been demonstrated. Frequency conversion with high efficiencies was realized by enhancement of the nonlinearity, where the pump is resonant with interband transitions, combined with a high terahertz intracavity power density. These developments show the potential of QCLs as novel optical components for future all-optical telecommunication networks.

## Methods

QCLs operating at 2.8 THz with GaAs/AlGaAs quantum wells and based on a bound-to-continuum design were used (thickness of active region, 12 μm). Samples were processed into a single plasmon geometry with a ridge width of 250 μm and cavity length of 1.5 mm. The samples were operated in c.w. mode at 10 K. (See Supplementary Section S1 for optical and electrical characteristics as well as the spectrum.) As the bandgap of GaAs is in the NIR, the interband pump was sourced from a c.w. Ti:sapphire laser that also allowed a large wavelength tunability and permitted the correct interband resonance excitation to be found. NIR pump power (100 μW) was used with a coupling efficiency of ~20%, resulting in ~20 μW being coupled into the QCL cavity. Low powers were used for the input NIR beam so as not to affect the QCL performance. This was verified by confirming that the threshold current observed in the change in differential resistance of the voltage-current (*VI*) curve did not increase with the coupled NIR beam. The transmitted NIR beam was collected at the opposite facet using a high-numerical-aperture objective and analysed using a spectrometer coupled to a thermoelectrically cooled CCD camera.

Received 18 January 2012; accepted 5 June 2012; published online 15 July 2012

## References


1. Eldada, L. Optical communication components. *Rev. Sci. Instrum.* **75,** 575–593 (2004).
2. Desurvire, E. Capacity demand and technology challenges for lightwave systems in the next two decades. *J. Lightwave Technol.* **24,** 4697–4710 (2006).
3. Campi, D. & Coriasso, C. Wavelength conversion technologies. *Photon. Network Commun.* **2,** 85–95 (2000).
4. Köhler, R. *et al.* Terahertz semiconductor–heterostructure laser. *Nature* **417,** 156–159 (2002).
5. DeCusatis, C., Maass, E., Clement, D. P. & Lasky, R. C. (eds) *Handbook of Fiber Optic Data Communication* (Academic Press, 1998).
6. Sirtori, C., Capasso, F., Faist, J., Pfeiffer, L. N. & West K. W. Far-infrared generation of doubly resonant difference frequency mixing in a coupled quantum well two dimensional electron gas system. *Appl. Phys. Lett.* **65,** 445–447 (1994).
7. Belkin, M. A. Terahertz quantum-cascade-laser source based on intracavity difference-frequency generation. *Nature Photon.* **1,** 288–292 (2007).
8. Kono, J. *et al.* Resonant terahertz optical sideband generation from confined magnetoexcitons. *Phys. Rev. Lett.* **79,** 1758–1761 (1997).
9. Černe, J. Near-infrared sideband generation induced by intense far-infrared radiation in GaAs quantum wells. *Appl. Phys. Lett.* **70,** 3543–3545 (1997).
10. Phillips, C., Su, M. Y., Sherwin, M. S., Ko, J. & Coldren, L. Generation of first-order terahertz optical sidebands in asymmetric coupled quantum wells. *Appl. Phys. Lett.* **75,** 2728–2730 (1999).
11. Carter, S. G. *et al.* Terahertz-optical mixing in undoped and doped GaAs quantum wells: from excitonic to electronic intersubband transitions. *Phys. Rev. B* **72,** 155309 (2005).
12. Ciulin, V., Carter, S. G., Sherwin, M. S., Huntington, A. & Coldren, L. A. Terahertz optical mixing in biased GaAs single quantum wells. *Phys. Rev. B* **70,** 115312 (2004).
13. Su, M. Y., Carter, S. G., Sherwin, M. S., Huntington, A. & Coldren, L. A. Voltage-controlled wavelength conversion by terahertz electro-optic modulation in double quantum wells. *Appl. Phys. Lett.* **81,** 1564–1566 (2002).
14. Wagner, M. *et al.* Resonant enhancement of second order sideband generation for intraexcitonic transitions in GaAs/AlGaAs multiple quantum wells. *Appl. Phys. Lett.* **94,** 241105 (2009).
15. Carter, S. G. *et al.* Terahertz electro-optic wavelength conversion in GaAs quantum wells: improved efficiency and room-temperature operation. *Appl. Phys. Lett.* **84,** 840–842 (2004).
16. Williams, B. S. Terahertz quantum cascade lasers. *Nature Photon.* **1,** 517–525 (2007).
17. Dhillon, S. S. *et al.* Terahertz transfer onto a telecom optical carrier. *Nature Photon.* **1,** 411–415 (2007).
18. Zervos, C. *et al.* Coherent near-infrared wavelength conversion in semiconductor quantum cascade lasers. *Appl. Phys. Lett.* **89,** 183507 (2006).
19. Barbieri, S. *et al.* 2.9 THz quantum cascade lasers operating up to 70 K in continuous wave. *Appl. Phys. Lett.* **85,** 1674–1676 (2004).
20. Rosencher, E. & Vinter B. *Optoelectronics* 2nd edn (Dunod, 2002).
21. Freeman, J. R., Brewer, A., Beere, H. E. & Ritchie, D. A. Photo-luminescence study of heterogeneous terahertz quantum cascade lasers. *J. Appl. Phys.* **110,** 013103 (2011).
22. Vitiello, M. S. *et al.* Measurement of subband electronic temperatures and population inversion in THz quantum cascade lasers. *Appl. Phys. Lett.* **86,** 111115 (2005).
23. Sutherland, R. L., McLean, D. G. & Kirkpatrick, S. *Handbook of Nonlinear Optics* (CRC Press, 2003).
24. Rosencher, E. & Bois, Ph. Model system for optical non-linearities: asymmetric quantum wells. *Phys. Rev. B* **44,** 011315 (1991).
25. Yariv, A. *Quantum Electronics* 3rd edn (Wiley, 1989).
26. Blakemore, J. S. Semiconducting and other major properties of gallium arsenide, *J. Appl. Phys.* **53,** R123–R181 (1982).
27. Garmire, E., Kost, A. & Khurgin, J. *Nonlinear Optics in Semiconductors II* (Academic Press, 1999).
28. Khurgin, J. Second-order nonlinear effects in asymmetric quantum-well structures. *Phys. Rev. B* **38,** 4056–4066 (1988).
29. Scalari, G. THz and sub-THz quantum cascade lasers. *Laser Photon. Rev.* **3,** 45–66 (2009).
30. Faist, J. Quantum cascade laser. *Science* **264,** 553–556 (1994).
31. Shin, W., Han, S. W., Park, C. S. & Oh, K. All fiber optical inter-band router for broadband wavelength division multiplexing. *Opt. Express.* **12,** 1815–1822 (2004).
32. Lu, Q. Y., Bai, Y., Bandyopadhyay, N., Slivken, S. & Razeghi, M. 2.4 W room temperature continuous wave operation of distributed feedback quantum cascade lasers. *Appl. Phys. Lett.* **98,** 181106 (2011).


## Acknowledgements

This work was financially supported by the Programme Francilien de Recherche en Nanosciences (CNano-IDF, contract TeraConversion) and the Agence Nationale de la Recherche (ANR, contract no. HI-TEQ ANR-09-NANO-017). J.R.F. acknowledges funding

from the Marie Curie Action fellowship (grant no. 274602). J.M. acknowledges funding from the French Ministry of Defense (DGA). Laboratoire Pierre Aigrain (LPA) is a Unité Mixte de Recherche Associée à l'ENS, of the Centre National de la Recherche Scientifique (CNRS) UMR8551 and of Universités Paris 6 and 7. Device fabrication was performed at the nanocentre La Centrale de Technologie Universitaire (CTU-IEF-Minerve), which is partially funded by the Conseil General de l'Essonne.

## Author contributions

J.M. and P.C. set up the experiment, acquired the experimental data and contributed equally to the work. S.S.D. conceived the experimental concept. Photoluminescence measurements were taken by J.R.F., K.M. and P.C. Sample growth was performed by H.E.B. and D.A.R. The manuscript was written and the data interpreted by J.M., P.C., J.R.F., N.J., J.M., J.T., C.S. and S.S.D. C.S. provided insight and interpretation of the nonlinear properties of QCLs. All work was coordinated and overseen by J.T. and S.S.D.

## Additional information

The authors declare no competing financial interests. Supplementary information accompanies this paper at www.nature.com/naturephotonics. Reprints and permission information is available online at http://www.nature.com/reprints. Correspondence and requests for materials should be addressed to S.S.D.